Metallophysics and Advanced Technologies
Металофіз. новітні технол.
Metallofiz. Noveishie Tekhnol.
2025, vol. 47, No. 11, pp. 1185–1198
https://doi.org/10.15407/mfint.47.11.1185
Reprints available directly from the publisher

PACS numbers: 61.72.Ff, 68.37.Hk, 68.43.Mn, 68.60.Dv, 81.15.Cd, 81.40.Gh, 81.65.Kn

Cobalt-Based Alloy Coating for Protecting Titanium from Hydrogen Permeation

V. A. Dekhtyarenko[*,**], T. V. Pryadko[*], V. V. Kyrylchuk[*], M. S. Nizameyev[*], V. I. Bondarchuk[*]

[*]*G. V. Kurdyumov Institute for Metal Physics, N.A.S. of Ukraine, 36 Academician Vernadsky Blvd., UA-03142 Kyiv, Ukraine*
[**]*E. O. Paton Electric Welding Institute, N.A.S. of Ukraine, 11 Kazymyr Malevych Str., UA-03150 Kyiv, Ukraine*

The microstructure and phase composition of a new-type protective coatings based on the Co–NbC system in as-deposited and annealed conditions are investigated with x-ray phase analysis and scanning electron microscopy. The coated titanium samples are annealed in a vacuum and in hydrogen atmosphere. Regardless of the atmosphere used, the protective coating is cracked during annealing, primarily due to the different coefficients of thermal expansion of the phases. An additional factor affecting this process is the decomposition of phases with a new phase formed in the coating during annealing, which is identified as aluminium oxide. As shown, the coating can withstand heating up to 500°C, but the exposure time should not exceed 20 min. Increasing the exposure time at this temperature (up to 120 min) lead to an active interaction of hydrogen with the substrate (titanium). As found out, the amount of hydrogen absorbed by the sample over the above-mentioned period of time is of ≅0.22 wt.% at an average rate of ≅0.0025 wt.%/min (for comparison, titanium iodide absorbs ≅1.40 wt.% over the same period of time).

Corresponding author: Volodymyr Anatoliiyovych Dekhtyarenko
E-mail: Devova@I.ua

Citation: V. A. Dekhtyarenko, T. V. Pryadko, V. V. Kyrylchuk, M. S. Nizameyev, and V. I. Bondarchuk, Cobalt-Based Alloy Coating for Protecting Titanium from Hydrogen Permeation, *Metallofiz. Noveishie Tekhnol.*, **47**, No. 11: 1185–1198 (2025), DOI: 10.15407/mfint.47.11.1185

Key words: titanium, hydrogen, cobalt-based alloy, protective coating, microstructure.

Методами рентґенівської фазової аналізи та сканувальної електронної мікроскопії досліджено мікроструктуру та фазовий склад нового типу захисних покриттів на основі системи Co–NbC у вихідному стані та після відпалу. Відпал титанових зразків із нанесеним покриттям було проведено у вакуумі та середовищі водню. Встановлено, що, незалежно від використаної атмосфери, під час відпалу відбулося розтріскування захисного покриття, в першу чергу, через ріжницю коефіцієнтів термічного розширення співіснуючих у ньому фаз. Додатковим чинником впливу на цей процес був розпад фаз, оскільки у структурі покриття під час відпалу утворилася нова фаза, яку було ідентифіковано як оксид Алюмінію. Показано, що дане покриття може витримувати нагрів до температури у 500°C, але водночас витримка має не перевищувати 20 хвилин. Збільшення часу витримки за вказаної температури (до 120 хвилин) привело до активної реакції взаємодії водню з основою (титаном). Визначено, що кількість увібраного зразком водню за вказаний проміжок часу становить ≅ 0,22 мас.% за середньої швидкости у ≅ 0,0025 мас.%/хв. (для порівняння: йодидний титан за аналогічний проміжок часу здатен увібрати ≅ 1,40 мас.%).

Ключові слова: титан, водень, стоп на основі кобальту, захисне покриття, мікроструктура.

(Received 19 June, 2025; in final version, 11 September, 2025)

1. INTRODUCTION

Hydrogen is considered as a clean and efficient energy source that is crucial for shaping a zero-emission future [1, 2]. Large-scale production, transportation, storage, and use of green hydrogen are expected to take place in the coming decades [3]. However, having the smallest atoms in the universe, hydrogen can adsorb, diffuse and interact with almost all metallic materials, thus degrading their mechanical properties [4–7]. This is especially true for titanium and titanium-based alloys [8, 9].

Titanium and Ti-based alloys are considered to be rather resistant to chemical corrosion. However, in many technological and commercial applications these materials are exposed to hydrogen-containing environments and, therefore, can be seriously affected due to hydrogen embrittlement [10–12], as they can absorb large amounts of hydrogen, especially at elevated temperatures [13, 14]. The degree of interaction of Ti-based alloys with hydrogen directly depends on their microstructure and chemical composition [15, 16]. According to [8], today there are four main ways to protect metals (including titanium) from interaction with hydrogen: formation of protective coatings on

the metal surface, which prevent the permeation of hydrogen into the bulk material [17]; alloying, which reduces the rate of interaction between the metal and the hydrogen-containing environment and increases the maximum acceptable hydrogen concentration [18]; modification of the material surface by high-energy impact [19]; annealing of the final products [20].

Despite the fact that the abovementioned methods of combating the negative effects of hydrogen on metallic materials have already found some application in industry, it is believed that the most promising way to solve this problem is still the use of protective coatings [17, 21–23]. The use of coatings, especially in nuclear and renewable energy, can extend the service life of materials by minimizing the negative impact of the interaction with hydrogen [24]. The methods for applying coatings are very diverse: electrolytic deposition of metals and alloys, gas transport reactions, ion implantation, chemical and thermal treatment, *etc.* [24, 25]. Their compositions are also diverse: oxides, borides, nitrides, carbides, silicides [26]. However, it was noted in Ref. [24] that although the existing coatings already meet certain technological requirements, it is still expedient to search for new approaches to the formation of protective layers with increased resistance to hydrogen permeation and other enhanced properties.

In Ref. [27], we first showed the prospects of using an alloy based on the Co–NbC system as a protective coating to counteract the negative impact of a hydrogen-containing environment on titanium. The 55.18Co–17.66Cr–12.18Nb–7.45W–3.07Fe–1.88Al–1.5C–1.59B [wt.%] alloy was studied. A technique for forming coatings was developed, which included: obtaining the alloy by induction melting; melt spinning (producing the ribbon); annealing the produced ribbon; milling the annealed ribbon; sieving powders of the needed fraction; plasma-enhanced deposition of the produced powders onto the titanium surface. The samples were annealed at 400°C and a hydrogen pressure of 0.6 MPa for 3.5 h. The sample did not react with hydrogen during this heat treatment. The present work is a continuation of the abovementioned work. The goal was to reveal possible changes in the structure and phase composition of the coating after heat treatment, as well as to determine the extreme service parameters for the formed coating.

2. EXPERIMENTAL/THEORETICAL DETAILS

The phase composition and lattice constants of the initial materials, as well as after annealing in hydrogen environment, were determined by means of x-ray phase analysis with a DRON-3M diffractometer. Metallographic studies were carried out with a VEGA3 TESCAN scanning electron microscope equipped with an XFlash610M EDS

detector (Bruker).

The sample with protective coating was annealed at 400°C for 3.5 hours in a vacuum furnace SShVE-1.25/25-I2 at a pressure of 10^{-3} MPa and a heating rate of ≅ 7°C/min.

The stability of the initial powders and the deposited protective coatings in a hydrogen environment was studied with the Sieverts method at an IVGM-2M unit [28, 29] at room temperature and during heating to 500°C (annealing at 400°C and 500°C was carried out in accordance with the data of Ref. [30]) at pressures 0.6–2.0 MPa. The amount of absorbed hydrogen was determined by the change in pressure in a closed volume (volumetric method) and additionally controlled by weighing with an accuracy of $1.5 \cdot 10^{-5}$ g (gravimetric method).

3. RESULTS AND DISCUSSION

As shown in Ref. [27], the protective coating on titanium was formed using the technique of plasma deposition in an argon flow. Argon was used for two reasons: (i) protection of partially or entirely molten powder from the negative effects of the environment (hydrogen, oxygen, and nitrogen); (ii) transportation of the powder to the substrate surface. The examination of microstructure of the protective coatings only on the surface of the samples would not allow obtaining complete information about the coating. Therefore, one sample was cut in half, which provided more information about the coating (Fig. 1).

As seen in Fig. 1, partial or complete melting of the powder particles occurred during the coating deposition, depending on the size of the initial powder. When deposited on the surface of titanium, the melted particles interacted with each other and partially with the substrate surface, which resulted in a rather high adhesion between the particles and the surface. The sufficient adhesion between the coating and the substrate, as well as between the particles, is proved by the absence of defects (cracks or delamination) at the interface between the substrate and the coating after mechanical impact on the sample (cutting, grinding, and polishing). Besides, it was found that the relief on the surface on which the protective layer was applied did not significantly affect the formation of the coating (Fig. 1, *c*). No intermediate layer between the substrate and the coating was observed (Fig. 1, *c*, *d*). This may indicate that the surface of the substrate did not significantly melt during the formation of the coating (this is important when depositing a coating on finished products).

The chemical compositions of the main phases (Table 1) in the studied coating were determined using the EDX technique. As was determined with the analysis of the coating surface [27], the basis of the deposited layer was a solid solution based on cobalt with

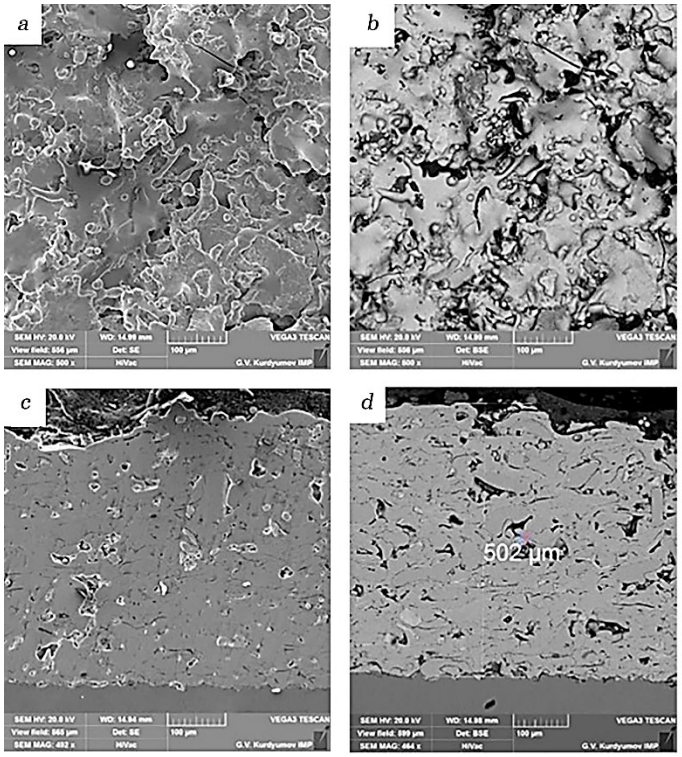

Fig. 1. Microstructure of protective coating: *a*, *b*—surface [27]; *c*, *d*—cross-section.

comparatively coarse inclusions of light-coloured niobium carbide of the NbC type (Fig. 1, *d*). The analysis of the coating cross section revealed a fairly uniform distribution of coarse niobium carbide particles (Fig. 1, *d*), which were present in the initial powders. The previous study of the coating surface [27] showed the absence of coarse carbide inclusions — only fine particles were observed (Fig. 1, *a*, *b*).

In Ref. [27], materials in their initial state, powders after heat treatment in hydrogen, and the deposited coating were studied using x-ray phase analysis (Table 2). Three phases were detected in the studied materials: Co-based solid solution, niobium carbide, and intermetallic compound $Cr_{0.7}Fe_{0.3}$. Using MAUD Software, we additionally examined the materials at each stage. This made it possible to reveal four phases in the structure, as well as to determine the volume fraction of each of them (Table 2).

According to MAUD Software, it was found that the volume fractions of the Co-based solid solution and niobium carbide were $\cong 76$ and $\cong 17.5\%$, respectively. Both phases have a face-centred cubic lattice of $Fm\text{–}3m$ space group. These data correlate with the literature

TABLE 1. Chemical compositions of phases in as-deposited coating.

Phase	Content, ±0.03 at.%								
	Co	Cr	Nb	W	Fe	Al	C	B	O
Solid solution	53.86	17.78	4.26	1.89	3.53	3.35	14.07	–	1.25
Niobium carbide	1.29	0.87	54.11	0.68	0.07	0.14	41.61	–	1.23

TABLE 2. Lattice constants of phases.

State	Lattice constants, ± 0.0009 (nm)				
	Co-based solid solution	NbC	$Cr_{0.7}Fe_{0,3}$	Co_2B	Al_2O_3
Initial powder [27]	a=0.3630	a=0.4406	a=0.2841	a=0.4909 c=0.4479	–
Powder annealed in hydrogen atmosphere [27]	a=0.3715	a=0.4433	a=0.2854	a=0.4831 c=0.4479	–
As-deposited coating [27]	a=0.3623	a=0.4490	a=0.2910	a=0.4914 c=0.4465	–
Coated sample after annealing in hydrogen atmosphere	a=0.3580	a=0.4480	a=0.2872	a=0.4993 c=0.4324	a=0.4760 c=1.2994

ones [31, 32] regarding the basis of alloys of this type. In addition to the abovementioned phases, the $Cr_{0.7}Fe_{0.3}$ intermetallic compound with a body-centred cubic lattice (volume fraction ≅3–4%) of the Im–$3m$ space group was also revealed. Besides, the Co_2B phase with a tetragonal lattice (volume fraction ≅2.5%) of the I–$42m$ space group was also found in the initial powder. The presence of this phase may be due to its incomplete dissolution during the production of the initial alloy, or its re-precipitation during melt solidification.

Comparison of the lattice constants (Table 2) of the phases at different stages (Table 2) showed a certain trend. Annealing in a hydrogen atmosphere led to a slight increase in the lattice constants, which was most likely due to some oxidation of the particles after contact with the atmosphere. This trend was also observed for most phases after coating deposition. On the contrary, the lattice constant of the Co-based solid solution slightly decreased below the initial value after coating deposition (Table 2). This can be explained by some redistribution of chemical elements with significant difference in atomic radius in the highly alloyed 55.18Co–17.66Cr–12.18Nb–7.45W–3.07Fe–1.88Al–1.5C–1.59B system [33], since the partial substitution of an alloy component with an element with a different

atomic radius is accompanied by changes in the volume of the unit cell [34].

According to the data of Ref. [27], after annealing at 400°C and a hydrogen pressure of 0.6 MPa for 3.5 h, there were no noticeable changes in the hydrogen pressure in the chamber, which indicated that there was no interaction between the sample and hydrogen. However, there was no simultaneous effect of temperature and hydrogen pressure on the coating [27]. According to SEM investigations, this treatment led to the formation of cracks in the coating (Fig. 2, *a*, *c*). It was found that the crack growth occurred not only along the interfaces between the particles, but also through their bulk (Fig. 2, *c*). This may indirectly indicate a fairly high adhesion between the particles. It was also found that the heat treatment in a hydrogen atmosphere led to the decomposition of the phases (Fig. 2, *a*). Dark-coloured crystallites appeared in the microstructure, which were identified as a phase based on aluminium oxide (Table 3). According to the literature [35], aluminium oxide can precipitate during annealing in the alloys based on Ni–NbC or Co–NbC systems.

X-ray phase analysis was performed to confirm the above conclusions regarding the change in the phase composition of the

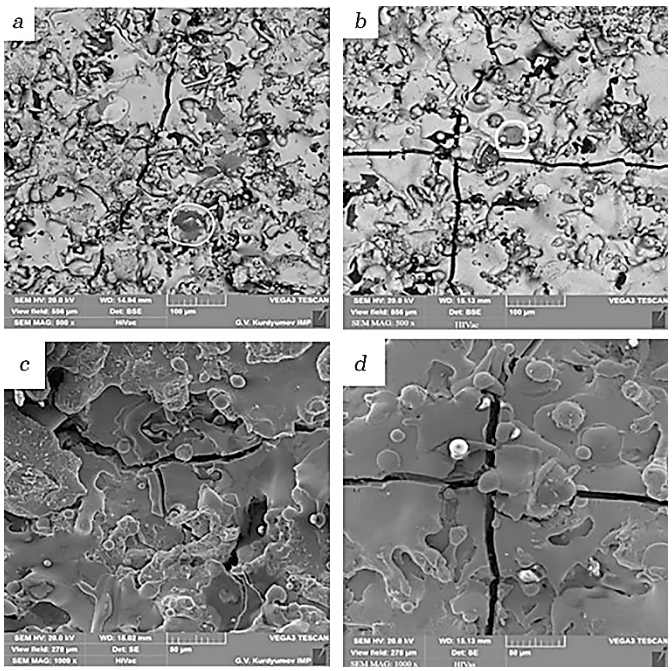

Fig. 2. Microstructure of coatings after annealing at 400°C: *a*, *c*—in a hydrogen atmosphere; *b*, *d*—in a vacuum.

TABLE 3. Chemical composition of dark-coloured crystallites precipitated upon annealing.

Environment	Content, ±0.03 at.%								
	Co	Cr	Nb	W	Fe	Al	C	B	O
Hydrogen	1.67	14.17	6.14	0.02	0.39	23.15	5.68	–	48.77
Vacuum	0.65	3.33	0.35	–	0.07	29.65	7.13	–	58.77

coating after annealing in a hydrogen environment (Table 2). As expected, the coating based on Co-based solid solution and niobium carbide of the NbC type formed upon annealing. Besides, Co_2B phase and $Cr_{0.7}Fe_{0.3}$ intermetallic compound remained. Beside the initial phases, a phase based on aluminium oxide with a trigonal lattice (volume fraction $\cong 10\%$) was detected. Comparison of the lattice constants of the phases in the initial state and after annealing in a hydrogen atmosphere showed that they somewhat decreased (Table 2). Most likely, this is associated with a decrease in the amount of oxygen in the phases due to the reducing effect of the hydrogen environment and the formation of a new phase based on aluminium oxide.

As shown above, after heating up to 400°C in a hydrogen atmosphere, cracks formed in the coating, but it is not clear whether this process was caused by hydrogen pressure, temperature, or their simultaneous action. Besides, the phase composition changed. At the same time, it was unclear where the oxygen came from in the amounts sufficient for this phase formation (Table 3). In order to clarify the causes of formation of cracks and the change in phase composition, annealing in vacuum was performed (at the same parameters). As a result, the effect of hydrogen pressure was discarded (Fig. 2, *b*, *d*). It was found that the vacuum annealing also led to the formation of cracks. As seen in Figs. 2, *a*, *c* and *b*, *d*, the linear dimensions of the cracks (first of all their widths) are similar. Besides, the following pattern was observed: the crack propagated not only along the interface between the particles (Fig. 2, *b*), but also through their volume, and the cracks are capable to bypass some particles (Fig. 2, *d*), thereby choosing the easiest way for its propagation. Figure 2, *b* also shows that dark-coloured crystallites (see Table 3) appeared in the coating after annealing in a vacuum. It should be noted that the amount of oxygen in this phase was higher after annealing in a vacuum than after heat treatment in a hydrogen atmosphere.

The results considered above indicate that the main factor that leads to the formation of cracks in the coating is the annealing temperature. Therefore, the difference in thermal expansion coefficients plays a decisive role in this process. However, it is still unclear what factor is determinant: the difference in thermal expansion coefficients between

the coating and the substrate, or between the phases in the coating. Hydrogen pressure does not significantly contribute to the process of crack nucleation and growth. It was also found out that the change in the phase composition of the protective coating was not affected by the atmosphere, in which it was annealed. Most likely, the corresponding change occurred due to diffusion processes in the coating under the impact of elevated temperature. It can be assumed that the difference in the amount of oxygen in the phase formed upon annealing in a vacuum and hydrogen atmosphere (Table 3) is associated with the reducing effect of hydrogen during the formation of this phase. It is well known that hydrogen can partially reduce oxide scale that is always present on the surface of metallic materials [36, 37].

As noted above, annealing at 400°C resulted in the formation of cracks in the coating, but no hydrogen absorption was detected. The next temperature chosen for annealing was 500°C; this temperature is considered optimal (range 400–600°C [38, 39]) for hydrogen saturation of titanium and b.c.c. Ti-based solid solutions. The same samples (which already had cracks) were studied to simulate real-world conditions of service.

As in previous experiments [27], at the first stage, the samples were kept at room temperature and a hydrogen pressure of 0.6 MPa for 192 hours (8 days). Exposure under these conditions did not lead to surface activation and, accordingly, to noticeable hydrogen absorption. The next step was heating to 500±10°C, holding at this temperature, and cooling to room temperature (Fig. 3).

The samples were heated to 410±5°C at a rate of ≅ 7 °C/min, and then from 410 to 500°C at a rate of only 2.0°C/min. The heating rate in the range 410–500°C was reduced based on the following considerations. Firstly, according to the literature [38, 39], the majority of elements

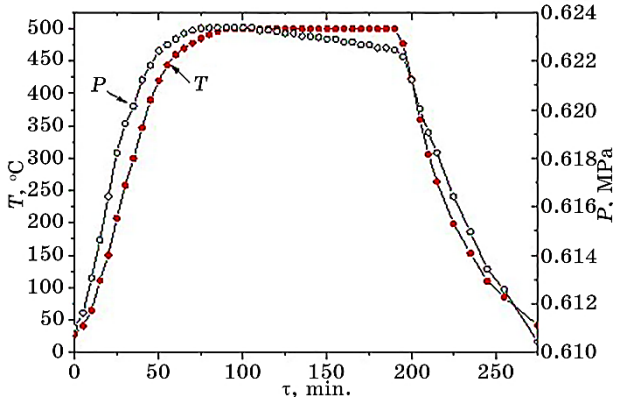

Fig. 3. Time dependences of hydrogen pressure and temperature.

that can actively absorb hydrogen (*e.g.*, Ti, Zr, Nb, and V) interact with the latter exactly in this temperature range. The second consideration was the presence of cracks that formed during heating to 400°C.

Time dependences of hydrogen pressure and temperature (Fig. 3) show no that no hydrogen absorption occurred during heating up to 500°C. The next step was to hold the sample at this temperature and hydrogen pressure of 0.622±0.02 MPa for 120 min. At the initial stage of exposure (≅30 min), no hydrogen absorption was detected; at further exposure (30–120 min), a rather active interaction began. The amount of hydrogen absorbed by the sample over this period of time was ≅0.22 wt.%, at an average rate of ≅0.0025 wt.%/min. This calculation was made not for the total mass of the sample, but only for the mass of the substrate, since, according to Ref. [27], the powders used to deposit the coating did not interact with hydrogen. According to Ref. [40], titanium iodide can absorb ≅1.40 wt.% at an average rate of ≅0.015 wt.%/min for a similar period of time (90 minutes) at a pressure of 0.5 MPa, starting from 450°C. The comparison of the amounts of hydrogen absorbed by iodide titanium [40] and the coated sample over the same period of time allows assuming that only some of the cracks that formed during the first heating reached the substrate.

Figure 4 shows the surface of the protective coating after annealing in a hydrogen atmosphere at different temperatures. The comparison of the microstructures allowed concluding that the main cause of the decreased catalytic capability of the coating after heating to 500°C was an increase in the linear dimensions of previously formed cracks and their coalescence with a continuous net formation (Fig. 4, *b*). As noted above, cracks formed in the coating (Fig. 4, *a*) upon annealing at 400°C, but the thickness of the protective layer was still sufficient to prevent the interaction of the substrate with hydrogen.

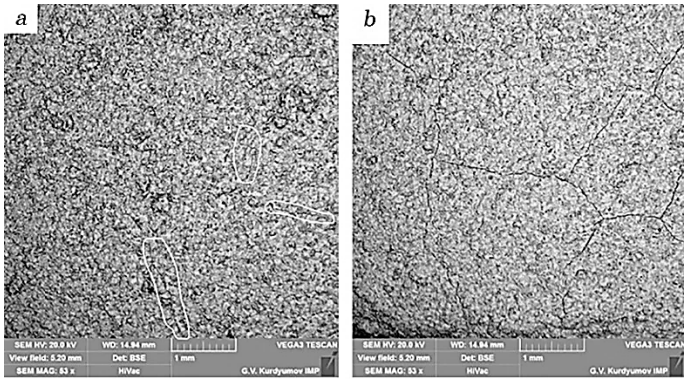

Fig. 4. Coating surface after annealing in hydrogen atmosphere at: *a*—400°C; *b*—500°C.

Figure 5 shows a cross section of the sample after annealing at 500°C. This made it possible to determine the degree of damage of the protective coating by its thickness (to clarify how the crack propagated), as well as changes in the substrate (whether the absorbed hydrogen permeated in titanium). As seen in Fig. 5, *a*, the second phase of dark colour with needle-like shape was observed in the substrate in the regions where the crack passed through the protective coating. We have previously determined [8, 40] that the hydride phase looks like this [8, 41]. To a certain extent, this confirms the calculations made above, according to which all the hydrogen that permeated the sample was dissolved in the substrate volume.

Comparison of the microstructures shown in Figs. 5, *a*, *b* showed that the linear dimensions of the cracks significantly affected the formation of the hydride phase in titanium. When the crack reaches the substrate, thin needles of the hydride phase form there (Fig. 5, *a*). Then the needles transform into a continuous layer of the hydride phase, and the coating around the crack fractures (Fig. 5, *b*). This can lead to delamination of the coating from the substrate due to an increase in the volume of the titanium unit cell and the high brittleness of the hydride phase [38]. It was also found out that the simultaneous effect of high temperature and

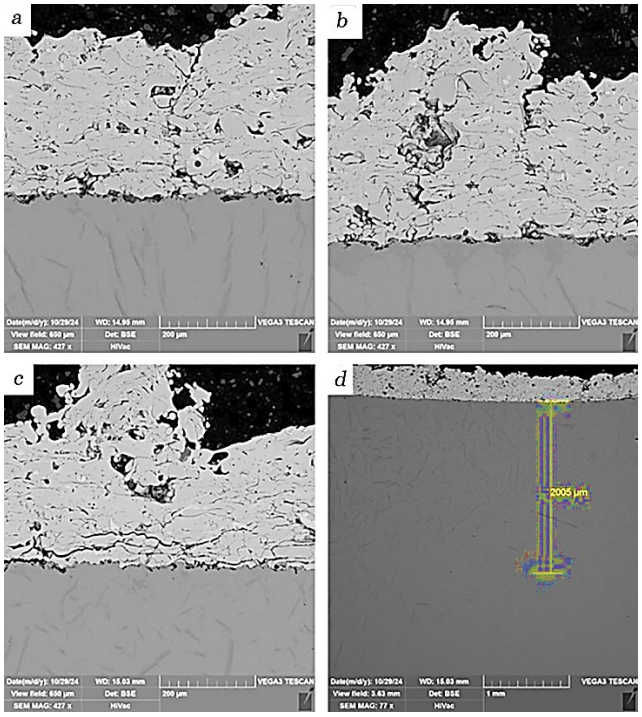

Fig. 5. Microstructure of sample annealed at 500°C.

TABLE 4. Chemical compositions of phases in coating after annealing.

Phase	Content, ±0.03 at.%								
	Co	Cr	Nb	W	Fe	Al	C	B	O
Gray	54.21	17.71	5.09	1.93	3.55	4.02	12.85	–	0.63
Light gray	1.22	0.73	55.44	0.53	0.06	0.14	40.55	0.33	1.00
Dark	3.78	9.84	2.94	0.06	0.37	25.96	6.03	–	51.03

hydrogen pressure led to the delamination of the coating (Fig. 5, *d*). Cracks up to 400 μm long formed, which propagated in the plane of the coating. These cracks grew mainly along the boundaries between the particles, and the particles located on the crack path were crashed. As a result, a whole area in the coating formed with practically zero adhesion between the particles and between the coating and the substrate. After 90 minutes of active absorption (hydrogen capacity was 0.22 wt.%), hydrogen diffused into the substrate volume to a depth of more than 2.0 mm (see Fig. 5, *d*). This phenomenon was observed on all sides of the sample, so the protective coating was damaged on all faces rather uniformly.

The chemical compositions of the main phases in the coating cross section are listed in Table 4. As noted above in the analysis of the coating surface, the basis of the deposited protective layer is the Co-based solid solution (gray phase) with comparatively coarse inclusions of light-coloured niobium carbide phase of NbC type. Beside these major phases, dark crystallites of the aluminium oxide formed after the first annealing. The chemical composition of the dark phase on the surface of the coating (Table 3) and in its depth (Table 4) was similar. The formation of aluminium oxide crystallites in the volume of the coating, to some extent, confirms the assumption made after annealing the sample in a vacuum that this phase precipitated due to diffusion processes in the coating at elevated temperatures.

X-ray phase analysis showed that five phases remained in the coating after annealing at 500°C (Table 2). The lattice constants of the phases, within the measurement errors, coincided with those after annealing at 400°C.

4. CONCLUSIONS

1. The annealing temperature is the main factor affecting the initiation of a crack in the coating and its further growth. The difference in thermal expansion coefficients of the coating and the substrate, as well as the phases in the coating, played a decisive role in this process. At the same time, the hydrogen pressure practically did not contribute to this process.

2. It is determined that phase decomposition in the protective coating can occur without the impact of the external atmosphere. A phase based on aluminium oxide formed due to diffusion processes that occurred in the coating annealed at elevated temperatures.
3. The protective coating from Co-based alloy allows heating titanium in a hydrogen atmosphere (pressure 0.6–0.62 MPa) up to 500±10°C (exposure time no more than 20 min) without a noticeable interaction between metal and hydrogen.

REFERENCES

1. S. W. Boettcher, *Chem. Rev.*, **124**, No. 23: 13095 (2024).
2. Y. C. Malede, A. Y. Adesina, F. Ashraf, and A. A. Sorour, *Renew Sustain Energy Rev*, **215**: 115528 (2025).
3. H. Yu, A. Dнaz, X. Lu, B. Sun, Y. Ding, M. Koyama, J. He, X. Zhou, A. Oudriss, X. Feaugas, and Z. Zhang, *Chem. Rev.*, **124**, No. 10: 6271 (2024).
4. O. Barrera, D. Bombac, Y. Chen, T. D. Daff, E. Galindo-Nava, P. Gong, D. Haley, R. Horton, I. Katzarov, J. R. Kermode, C. Liverani, M. Stopher, and F. Sweeney, *J Mater Sci.*, **53**: 6251 (2018).
5. M. L. Martin, M. Dadfarnia, A. Nagao, S. Wang, and P. Sofronis, *Acta Mater.*, **165**: 734 (2019).
6. V. G. Gavriljuk, V. M. Shyvaniuk, and S. M. Teus, *Hydrogen in Engineering Metallic Materials* (Cham: Springer: 2022).
7. P. Cavaliere, *Hydrogen Embrittlement in Metals and Alloys* (Cham: Springer: 2025).
8. V. A. Dekhtyarenko, T. V. Pryadko, O. I. Boshko, V. V. Kirilchuk, H. Yu. Mykhailova, and V. I. Bondarchuk, *Prog. Phys. Met.*, **25**, No. 2: 276 (2024).
9. P. Cavaliere, *Hydrogen Embrittlement in Metals and Alloys* (Cham: Springer: 2025).
10. M. B. Djukic, G. M. Bakic, V. S. Zeravcic, A. Sedmak, and B. Rajicic, *Corrosion*, **72**, No. 7: 943 (2016).
11. D. Oryshych, V. Dekhtyarenko, T. Pryadko, V. Bondarchuk, and D. Polotskiy, *Machines. Technologies. Materials*, **13**, No. 12: 561 (2019).
12. M. Hao, Y. Fu, Q. Hu, X. Lu, H. Zhang, Y. Ba, Y. Xie, K. Liu, and D. Li, *J. Ind. Eng. Chem.*, **145**: 491 (2025).
13. V. A. Dekhtyarenko, D. G. Savvakin, V. I. Bondarchuk, V. M. Shyvanyuk, T. V. Pryadko, and O. O. Stasiuk, *Prog. Phys. Met.*, **22**, No. 3: 307 (2021).
14. V. A. Dekhtyarenko, T. V. Pryadko, T. P. Vladimirova, C. V. Maksymova, O. M. Semyrga, and V. I. Bondarchuk, *Prog. Phys. Met.*, **25**, No. 4: 765 (2024).
15. E. Tal-Gutelmacher and D. Eliezer, *Glass. Phys. Chem.*, **31**: 96 (2005).
16. B. J. M. Freitas, A. L. Vidilli, A. B. Guerra, D. C. F. Ferreira, A. H. Kasama, M. T. P. Paes, G. Y. Koga, and C. Bolfarini, *J. Alloys Compds.*, **1019**: 179258 (2025).
17. M. Wetegrove, M. J. Duarte, K. Taube, M. Rohloff, H. Gopalan, C. Scheu, G. Dehm, and A. Kruth, *Hydrogen*, **4**, No. 2: 307 (2023).
18. O. M. Ivasyshyn, D. H. Savvakin, V. A. Dekhtyarenko, and O. O. Stasyuk, *Mater. Sci.*, **54**: 266 (2018).

19. Q. Xu and J. Zhang, *Sci Rep.*, **7**: 16927 (2017).
20. W. Yang, E. Hwang, H. Kim, S. Ahn, S. Kim, and H. Castaneda, *Surf. Coat. Technol.*, **378**: 124911 (2019).
21. M. Tamura and T. Eguchi, *J Vac. Sci. Technol.*, **A33**: 0415031 (2015).
22. D. I. Cherkez, A. V. Spitsyn, A. V. Golubeva, O. I. Obrezkov, S. S. Ananyev, N. P. Bobyr, and V. M. Chernov, *Phys. Atom. Nuclei*, **82**: 1010 (2019).
23. J. Liu, Y. Guo, X. Xing, X. Zhang, Y. Yang, and G. Cui, *Int. J. Hydrogen Energy*, **101**: 504 (2025).
24. C. E. E. Rönnebro, R. L. Oelrich, and R. O. Gates, *Molecules*, **27**, No. 19: 6528 (2022).
25. E. M. Rudenko, M. V. Dyakin, I. V. Korotash, D. Yu. Polotskiy, and V. A. Dekhtyarenko, *Metallofiz. Noveishie Tekhnol.*, **47**, No. 7: 703 (2025).
26. G. D. Tolstolutska, G. D. Tolstolutska, M. O. Azarenkov, V. A. Bilous, O. S. Kuprin, and M. G. Ishchenko, *Probl. Atomic Sci. Technol.*, **152**, No. 4: 100 (2024).
27. V. Dekhtyarenko, I. Zagorulko, O. Boshko, T. Pryadko, V. Kyrylchuk, O. Semyrga, I. Evlash, D. Stepanov, and V. Bondarchuk, *Materials Science. Non-Equilibrium Phase Transformations*, **10**, No. 1: 33 (2024).
28. H. Y. Mykhailova, V. A. Dekhtyarenko, and Y. V. Vasylyk, *MRS Communications*, **13**: 1288 (2023).
29. V. A. Dekhtyarenko, *MRS Communications*, **14**: 337 (2024).
30. V. Nemanič, *Nucl. Mater. Energy*, **19**: 451 (2019).
31. T. S. Cherepova, G. P. Dmitrieva, A. V. Nosenko, and A. M. Semirga, *Science and Innovation*, **10**, No. 4: 20 (2014).
32. G. P. Dmitrieva, T. S. Cherepova, and T. V. Pryadko, *Prog. Phys. Met.*, **22**, No. 4: 678 (2021).
33. N. N. Greenwood and A. Earnshaw, *Chemistry of the Elements. 2nd Ed.* (Oxford: Butterworth Heinemann: 1997).
34. V. A. Dekhtyarenko, T. V. Pryadko, T. P. Vladimirova, S. V. Maksymova, H. Yu. Mykhailova, and V. I. Bondarchuk, *Prog. Phys. Met.*, **25**, No. 3: 520 (2024).
35. G. P. Dmytrieva, T. S. Cherepova, T. V. Pryadko, and Yu. S. Semenova, *MRS Communications*, **15**: 99 (2025).
36. V. G. Ivanchenko, V. A. Dekhtyarenko, and T. V. Pryadko, *Metallofiz. Noveishie Tekhnol.*, **37**, No. 4: 521 (2015).
37. O. M. Ivasishin, D. G. Savvakin, M. M. Gumenyak, and A. B. Bondarchuk, *Key Eng. Mater.*, **520**: 121 (2012).
38. V. A. Dekhtyarenko, D. G. Savvakin, O. O. Stasiuk, and D. V. Oryshych, *Metallofiz. Noveishie Tekhnol.*, **44**, No. 7: 887 (2022).
39. O. M. Ivasyshyn and D. H. Savvakin, *Mater. Sci.*, **51**: 465 (2016).
40. T. V. Pryadko, V. A. Dekhtyarenko, V. I. Bondarchuk, M. A. Vasilyev, and S. M. Voloshko, *Metallofiz. Noveishie Tekhnol.*, **42**, No. 10: 1419 (2020).
41. T. V. Pryadko, V. A. Dekhtyarenko, and A. A. Shkola, *Mater. Sci.*, **56**: 75 (2020).